University of Sistan and Baluchestan

Journal of Epigenetics

Online ISSN: 2676 - 4350

Homepage: https://jep.usb.ac.ir

Iranian Genetics Society

Role of P450 in the detoxification of pesticides with special references on Plutella xylostella resistance using bioinformatic analysis; Accepted

Mahdiyeh Poodineh Moghadam Jahantigh [1], Soltan Ravan [1], Ali R. Bandani [2*], Abbasali Emamjomeh [3]

[1] Department of Plant Protection, Faculty of Agriculture, Zabol University, Zabol, Iran. E-mail: Mahdiyehpoodineh5829@gmail.com , Ravan@gmail.com

[2] *Corresponding author*, Plant Protection Department, College of Agriculture and Natural Resources, University of Tehran, Iran. E-mail: abandani@ut.ac.ir

[3] Department of Agriculture and Plant Breeding, Faculty of Agriculture, Zabol University, Zabol, Iran. E-mail: aliimamjomeh@uoz.ac.ir

ARTICLE INFO

Article type:
Research Article

Article history:
Received:10 February 2026
Revised:23 Februaey 2026
Accepted:28 February 2026

Keywords:
CYP321E1,
CYP9G2,
metabolic resistance,
lepidopteran cytochrome P450,
regional differentiation.

A B S T R A C T

The diamondback moth, Plutella xylostella, is notorious for rapid evolution of resistance, often implicating cytochrome P450–mediated detoxification in control failures. This study evaluated whether geographically distinct Iranian populations exhibit consistent or divergent transcriptional responses of two candidate P450 genes following exposure to two widely used insecticide classes. We compared three field populations after exposure to acetamiprid (neonicotinoid) and cypermethrin (pyrethroid) and quantified time-dependent transcript changes in CYP321E1 and CYP9G2 at 48 h and 72 h, complemented by phylogenetic placement of both loci to contextualize sequence relatedness. CYP321E1 showed pronounced and sustained induction in the Arak population under both insecticides (≈22–68-fold after acetamiprid and ≈50–59-fold after cypermethrin across 48–72 h), whereas Karaj displayed intermediate induction with marked attenuation at 72 h under cypermethrin, and Qazvin exhibited a stronger response to acetamiprid than to cypermethrin with declining expression at 72 h. CYP9G2 responses were heterogeneous: Qazvin showed robust induction across insecticides and time points, Arak exhibited a transient increase primarily under cypermethrin at 48 h with minimal late response, and Karaj showed its clearest induction at 72 h under cypermethrin. Phylogenetic reconstructions supported clearer near-neighbor placements but weakly resolved deeper relationships, consistent with rapid P450 diversification. Collectively, these findings indicate population-specific detoxification transcriptional architectures and nominate CYP321E1/CYP9G2 as region-sensitive candidate markers to prioritize for functional validation and resistance monitoring

Introduction

The diamondback moth, Plutella xylostella (L.), is a globally important crucifer pest with an exceptional capacity to evolve insecticide resistance, frequently compromising field control. Because local spray histories and gene flow can create strong geographic heterogeneity, resistance mechanisms and molecular markers may differ among nearby populations. Here, we test whether

DOI: https://doi.org/10.22111/jep.2026.54742.1106

Publisher: University of Sistan and Baluchestan

How to Cite: Poodineh Moghadam Jahantigh, M., Ravan, S., Bandani, Ali.R., & Emamjomeh, A. (2026). Role of P450 in the detoxification of pesticides with special references on Plutella xylostella resistance using bioinformatic analysis; Accepted. *Journal of Epigenetics*, 7(1), 28-43. https://doi.org/10.22111/jep.2026.54742.1106

three Iranian field populations exhibit divergent transcriptional responses of two candidate cytochrome P450 genes following exposure to two widely used insecticide classes (acetamiprid and cypermethrin), aiming to identify region-informative candidates for resistance monitoring (Furlong et al., 2013; You et al., 2013; Sparks & Nauen, 2015; Banazeer et al., 2022).

Among the insecticide groups used against P. xylostella, neonicotinoids (e.g., acetamiprid) and pyrethroids (e.g., cypermethrin) remain operationally relevant in many production systems due to their cost, accessibility, and broad-spectrum activity. These compounds act on distinct neural targets: neonicotinoids modulate nicotinic acetylcholine receptors, while pyrethroids disrupt voltage-gated sodium channel function (Casida & Durkin, 2013; Soderlund, 2008). Yet, despite this mechanistic separation at the target site, resistance often emerges through convergent physiological solutions—particularly enhanced detoxification—allowing populations to tolerate multiple chemistries and thereby eroding the effectiveness of rotation schemes (Sparks & Nauen, 2015). In practice, the resulting "selection mosaic" can generate pronounced geographic differences in resistance profiles over relatively short spatial scales, especially where local spray regimes, crop phenology, and immigration pressures differ among regions (Banazeer et al., 2022). These realities motivate region-specific, mechanistically informed surveillance, not only to document resistance status but also to identify molecular markers that can forecast resistance trajectories before control failure becomes widespread.

Metabolic resistance—where detoxification enzymes reduce the internal dose of an insecticide before it reaches its target—has become a dominant mechanism across insect taxa, and in Lepidoptera it is frequently mediated by cytochrome P450 monooxygenases (P450s) (Dermauw et al., 2020; Nauen et al., 2022; You et al., 2013). P450s constitute a large and rapidly evolving superfamily, typically organized into clans and families with extensive gene duplication, loss, and functional diversification, especially in lineages facing diverse xenobiotic environments (Dermauw et al., 2020). This evolutionary plasticity has practical consequences: (i) closely related species, and even conspecific populations, can differ substantially in the composition and inducibility of P450 repertoires; and (ii) resistance can arise either through quantitative changes (e.g., elevated expression) or qualitative changes (e.g., amino-acid substitutions affecting catalytic properties), often shaped by local selection histories (Nauen et al., 2022).

In P. xylostella, genomic and transcriptomic resources have clarified the scale of the detoxification toolkit and revealed frequent upregulation of detoxification genes in resistant strains or following insecticide exposure (Lin et al., 2013; Yu et al., 2015; You et al., 2013). However, translating these broad patterns into actionable, population-level inference remains challenging. First, transcriptional responses can be highly context-dependent: induction profiles depend on insecticide class, dose, exposure route, developmental stage, and sampling time, with some genes responding transiently and others showing sustained elevation (Nauen et al., 2022; Ye et al., 2022). Second, population heterogeneity can be substantial even within a single country, reflecting localized insecticide use and demographic processes such as immigration and founder effects (Banazeer et al., 2022). Third, expression differences alone do not prove causal metabolic function; functional validation (e.g., RNAi, heterologous expression, synergist bioassays) is typically required to confirm whether a candidate P450 contributes to resistance (Nauen et al., 2022). Nevertheless, targeted expression profiling remains a powerful and practical first step for identifying candidate resistance markers and for prioritizing P450s for downstream functional and biochemical work, particularly where resources constrain genome-wide approaches.

Within Lepidoptera, several P450 families repeatedly appear in resistance research, including members of the CYP3 clan (e.g., the CYP6 and CYP9 families), which commonly metabolize xenobiotics and are often inducible (Dermauw et al., 2020; Nauen et al., 2022). In P. xylostella, CYP321E1 has been reported as a candidate detoxification gene and experimentally implicated in resistance-related phenotypes via gene knockdown during diamide exposure, highlighting its potential functional relevance in xenobiotic response pathways (Hu et al., 2014). Although CYP321E1 is not universally "the" resistance gene across populations and insecticides, its inducibility and demonstrated contribution in at least one

insecticide context justify evaluating it under alternative selection regimes and chemistries, including those that remain widely used for field control.

CYP9-family genes, including CYP9G2, are also of strong interest because CYP9 subfamily members are frequently associated with detoxification of plant allelochemicals and synthetic insecticides in Lepidoptera and can display robust inducibility after xenobiotic exposure (Dermauw et al., 2020; Nauen et al., 2022). Genome-wide analyses and expression profiling in P. xylostella reinforce the broader view that CYP9 genes are among the detoxification-associated candidates responsive to chemical stress, although the precise gene(s) involved can vary among populations and insecticide classes (Yu et al., 2015; You et al., 2013). Importantly, different insecticides can elicit distinct transcriptional signatures: a gene that is informative under one chemical may be unresponsive under another, and the same gene can show diverging time-course behavior among populations exposed to different selection histories (Ye et al., 2022). Therefore, testing CYP321E1 and CYP9G2 under both neonicotinoid and pyrethroid exposure provides a conceptually strong framework for understanding whether Iranian field populations exhibit gene- and insecticide-specific transcriptional responses that could plausibly reflect differential selection.

Despite substantial progress in mapping detoxification gene families and documenting resistance in P. xylostella, several gaps still exist, particularly in translating molecular insights into regionally actionable resistance monitoring. First, many studies contrast a single resistant strain with a susceptible laboratory reference, which is valuable mechanistically but less informative for understanding the range of molecular responses among contemporary field populations that may differ in pesticide exposure histories and genetic background (Banazeer et al., 2022; Nauen et al., 2022). Second, time-course data are often limited, yet temporal dynamics can be mechanistically revealing: rapid but transient induction may indicate a short-lived stress response, whereas sustained elevation may reflect regulatory rewiring or stable selection favoring higher constitutive or prolonged expression (Ye et al., 2022). Third, expression-based evidence is strengthened when integrated with sequence-level analyses. Because P450 families evolve through duplication and divergence, phylogenetic context can help interpret whether candidate genes fall into lineages enriched for xenobiotic metabolism, while population genetic signals (e.g., haplotype structure and neutrality statistics) can provide preliminary evidence about whether local selection may have acted on the locus or linked regions (Dermauw et al., 2020; Nauen et al., 2022). Although such analyses do not, by themselves, prove functional resistance mechanisms, they can sharpen mechanistic hypotheses and guide efficient prioritization for functional validation.

Against this backdrop, the present study was designed to quantify the transcriptional responses of two candidate detoxification-associated cytochrome P450 genes, CYP321E1 and CYP9G2, following exposure to acetamiprid and cypermethrin in three geographically distinct P. xylostella field populations from Iran: Arak (P1), Karaj (P2), and Qazvin (P3). Relative transcript abundance was measured at 48 h and 72 h post-exposure, with expression normalized to actin and calculated using the 2^−ΔΔCt framework.

This sampling structure was selected to capture both intermediate and later transcriptional states after insecticide challenge, enabling inference about whether induction is sustained or decays over time (Ye et al., 2022). In parallel, the study placed P. xylostella CYP321E1 and CYP9G2 sequences into a broader phylogenetic context and examined sequence variation patterns to support the interpretation of population differences and evolutionary constraints (Dermauw et al., 2020; Nauen et al., 2022).

The study was guided by three testable hypotheses. First, we hypothesized that exposure to acetamiprid and cypermethrin would elicit measurable transcriptional modulation of CYP321E1 and/or CYP9G2, consistent with inducible xenobiotic response networks observed in Lepidoptera, including P. xylostella (Yu et al., 2015; You et al., 2013). Second, we hypothesized that the magnitude and direction of these responses would differ among the three field populations, reflecting spatially variable selection pressures and genetic backgrounds shaped by local management histories and demographic processes (Banazeer et al., 2022; Nauen et al., 2022). Third, we hypothesized that sequence-level analyses would

provide complementary context—via phylogenetic placement and population genetic summaries—supporting refined hypotheses about whether observed expression patterns could plausibly align with local selection on detoxification pathways or with broader evolutionary dynamics of P450 gene families (Dermauw et al., 2020; Nauen et al., 2022).

The novelty of this work lies in its integrated, population-comparative design that evaluates two candidate P450 genes across two widely used insecticide classes and across multiple field populations, using a time-structured post-exposure sampling scheme.

By explicitly linking population identity, insecticide class, and transcriptional time course, the study aims to move beyond single-strain contrasts toward a framework that better reflects the heterogeneity encountered in real production systems (Sparks & Nauen, 2015; Banazeer et al., 2022). From a practical standpoint, identifying consistent, population-informative expression signatures can support hypothesis-driven resistance monitoring and can help prioritize candidate genes for functional validation—an essential step for converting molecular correlates into causal evidence (Nauen et al., 2022). More broadly, the combined expression and sequence-based perspective help interpret candidate-gene patterns within the dynamic evolutionary landscape of P450 families, where gene turnover and regulatory diversification complicate generalization across regions (Dermauw et al., 2020). Ultimately, insights from this study can inform locally grounded insecticide resistance management strategies, including evidence-based choices of rotation partners and the design of molecular surveillance panels tailored to the most relevant resistance pathways in Iranian P. xylostella populations (Sparks & Nauen, 2015).

Materials and methods

Insect collection, colony establishment, and rearing conditions

Larvae of the diamondback moth, *Plutella xylostella* (L.) (Lepidoptera: Plutellidae), were collected from cabbage-producing areas in three provinces of Iran: Arak (34°04′16.6″N, 49°48′47.9″E), Alborz/Karaj (35°46′59.6″N, 50°55′04.2″E), and Qazvin (36°15′12.6″N, 49°56′50.2″E). Field-collected larvae were transported to the Zabol Research Institute laboratory and reared for two generations on white cabbage under controlled conditions. Colonies from each geographic origin were maintained separately in enclosed net cages (60 × 60 × 90 cm) at 25 °C under an 8:16 h dark: light photoperiod.

Insecticides and bioassays

Two insecticides were evaluated: cypermethrin (EC 40%; Green Spectrum Products Co.) and acetamiprid (20% SP; Plant Co.). Acute toxicity was assessed using a leaf immersion bioassay with 3-day-old third instar larvae, following a standard arthropod bioassay framework. For each insecticide, five test concentrations were selected after preliminary range-finding to target an approximate 25–75% mortality range. White cabbage seedling leaves were excised; petioles were wrapped with wet cotton and aluminum foil to maintain turgor during exposure. Leaves were immersed in insecticide solution for 30 s and then air-dried at room temperature. Control leaves were treated with water containing Tween emulsifier (0.02%). Larvae were starved for 2 h before exposure. Ten larvae were placed in each Petri dish containing treated leaf tissue, and the dishes were sealed with a ventilated lid. Mortality was scored at 48 h and 72 h post-exposure, and the same time points were used to sample larvae for gene-expression analysis (Amiri and Bandani, 2013; Farahani et al., 2020).

RNA extraction, DNase treatment, and cDNA synthesis

At 48 h and 72 h following exposure, larvae were collected for molecular assays. Total RNA was extracted using a column-based RNA extraction kit (Denazist, Iran). RNA integrity was assessed by electrophoresis on a 1% agarose gel, and RNA quantity/quality were assessed spectrophotometrically (NanoDrop™ 1000; Thermo Scientific, USA) by absorbance at 230, 260, and 280 nm. To remove residual genomic DNA, RNA was treated with DNase (Fermentas, USA) at 37 °C for 30 min, followed by inactivation with EDTA. For first-strand cDNA synthesis, RNA was combined with oligo(dT) and random primers and adjusted to volume with DEPC-treated water, incubated at 65 °C for 10 min to disrupt secondary structures, and then reverse transcribed using a reverse transcription kit (SMOBio, Taiwan) at 42 °C for 90 min. Reactions were

terminated at 70 °C for 5 min, and cDNA was stored at −80 °C until use (Amiri et al., 2015).

Primer design and RT–qPCR

Primers were designed in Geneious R23 and evaluated using OligoAnalyzer; specificity was verified by Primer-BLAST against NCBI/GenBank. Target genes were CYP321E1 (accession KC626090; 94 bp amplicon; forward 5′-CTGGCTCACATTCTACGCAAC-3′, reverse 5′-TGGCAGGTCTTATGATGAGGG-3′) and CYP9G2 (accession AB096739; 147 bp; forward 5′-TGGTGGGAAACTCTTTGACGA-3′, reverse 5′-TGTTTTCGCGATGCTGCATAG-3′). Actin was used as the internal reference gene (accession NM_001309126; 128 bp; forward 5′-CCGTGCCCATCTACGAAGGTTA-3′, reverse 5′-AGCGGTGGTGGTGAAGGAGTATC-3′).

Quantitative PCR was performed on an ABI StepOne Real-Time PCR system (Applied Biosystems, USA) using SYBR Green chemistry (Ampliqon; 2× SYBR Green High ROX). Each reaction was run in a final volume of 10 µL containing 5 µL of 2× SYBR Green master mix and 2 µL of cDNA template. Thermocycling was: 94 °C for 15 min, followed by 40 cycles of 95 °C for 15 s, 59 °C for 40 s, and 72 °C for 20 s (Rahmani and Bandani, 2020).

Relative transcript abundance was calculated using the 2^−ΔΔCt method (Schmittgen & Livak, 2008; Alborzi et al., 2025), with actin as the internal control. Expression values were summarized as mean ± SE.

Phylogenetic reconstruction

Phylogenetic analyses were conducted separately for CYP321E1 and CYP9G2 to contextualize each target sequence within homologous P450 lineages. Homologous coding sequences were retrieved from the NCBI Nucleotide database using accession-guided searches. Multiple sequence alignment was performed using ClustalW, and phylogenetic inference was conducted in MEGA 7 using the Neighbor-Joining (NJ) method. Node support was evaluated using bootstrap resampling with 10,000 replicates, and bootstrap percentages were displayed at each node. All accessions included in each reconstruction were reported in the relevant figure (Alborzi et al., 2025).

Heatmap visualization of expression profiles

To summarize transcriptional responses across populations, insecticides, and time points, heatmaps were generated separately for CYP321E1 and CYP9G2 using $\log_2$-transformed fold-change values derived from RT–qPCR (2^−ΔΔCt outputs). Because fold-change data are inherently relative to the calibrator, the control condition was represented as $\log_2$(fold-change) = 0 for each population, and treatment cells were plotted as $\log_2$(fold-change) values. Heatmap matrices were arranged with treatments/time combinations as rows (Control; acetamiprid 48 h; acetamiprid 72 h; cypermethrin 48 h; cypermethrin 72 h) and populations as columns (P1–P3). Values were not converted to z-scores in the final figures unless explicitly stated, because z-scoring alters the quantitative interpretation by rescaling each population's dynamic range (Alborzi et al., 2025).

Statistical analysis of gene-expression data

Gene-expression data were analyzed in SPSS v22.0 (IBM Statistics). Differences among treatments within each population were tested using one-way ANOVA followed by Tukey's post hoc test, with $p < 0.05$ considered statistically significant. Statistical significance in tables was indicated by different lowercase letters within each population column, with means sharing the same letter not significantly different at $p < 0.05$ (Alborzi et al., 2025).

Results

Phylogenetic relationships of Plutella xylostella CYP321E1 among lepidopteran P450 lineages A phylogenetic reconstruction based on cytochrome P450 (CYP) coding sequences (CDS) from representative Lepidoptera resolved multiple, clearly separated terminal groupings, while several deeper nodes remained weakly supported (Figure 1). Within this topology, the *Plutella xylostella* sequence (KC626090.1; CYP321E1) was placed in a small cluster with *Hyphantria cunea* (ON032366.1), supported by a node value of 40. In contrast, many internal bifurcations across the tree backbone showed very low support values (often ≤16, and in several cases 0), indicating limited resolution of deeper relationships among the included CYP lineages under the present sequence

set and inference settings. Terminal associations were nonetheless visible, including a closely grouped pair of *Chilo suppressalis* (MN010765.1) and *Leucinodes orbonalis* (PP987297.1) with a node value of 31, and a distinct grouping of *Athetis lepigone* (OR373044.1) with *Pieris rapae* (KY212076.1) supported by a node value of 16. Branch lengths were drawn to scale (Figure 1), reflecting measurable divergence among taxa and contributing to the separation of multiple lineages across the tree. Overall, Figure 1 positions *P. xylostella* CYP321E1 within a lepidopteran comparative framework, with its nearest displayed neighbor being *H. cunea* under moderate support, whereas the broader branching order among several lineages remains weakly supported.

Broad-scale placement of Plutella xylostella CYP321E1 across insects

To further contextualize the taxonomic placement of *P. xylostella* CYP321E1, a second phylogeny was constructed using CYP CDS from a wider range of insects (Figure 2). Several terminal clades were recovered with strong bootstrap support. Notably, *Chilo suppressalis* (MN010765.1) and *Spodoptera exigua* (KX443477.1) formed a highly supported pair (bootstrap = 100), which grouped with *Apis mellifera* (DQ244074.1) under similarly strong support (bootstrap = 100). *Aedes aegypti* (AY947549.1) and *Bombyx mori* (AB198340.1) formed another well-supported pairing (bootstrap = 100). Additional strongly supported terminal relationships included *Anopheles gambiae* (KF656700.1) with *Sitophilus oryzae* (MN635144.1) (bootstrap = 100), and *Drosophila melanogaster* (AY138853.1) with *Helicoverpa armigera* (KR709085.1) (bootstrap = 100). In the mid-to-lower portion of the tree, *Bemisia tabaci* (PP239341.1) grouped with *Tenebrio molitor* (KP859376.1), with the relevant internal support shown as 67 (Figure 2). Importantly for the target sequence, *P. xylostella* (KC626090.1) was placed in a basal grouping with *Locusta migratoria* (KY009922.1) and *Leptinotarsa decemlineata* (KF044272.1), supported by a bootstrap value of 95 at the corresponding node, indicating a stable placement of these taxa as a cluster in this analysis. The deeper split separating major groups displayed comparatively weaker support (bootstrap = 48; Figure 2), consistent with reduced confidence in the backbone ordering relative to the strongly supported terminal groupings. Genetic distances are indicated by the scale bar (0.10 substitutions per site), reflecting substantial divergence across the included CYP sequences (Figure 2).

Phylogenetic relationships of Plutella xylostella CYP9G2 among lepidopteran P450 lineages

A Neighbor-Joining phylogeny based on coding sequences placed the *Plutella xylostella* CYP9G2 sequence (AB458853.1) on a distinct terminal branch that is separated from the remaining lepidopteran taxa included in the analysis (Fig. 3; scale bar = 0.10 substitutions per site). In contrast to several strongly supported terminal groupings elsewhere in the tree, the immediate placement of AB458853.1 relative to the closest included lineages is not annotated with a high bootstrap value on the internal node(s) adjacent to this branch, indicating that its local branching position is not among the most strongly supported relationships displayed in this figure.

Within Lepidoptera, multiple pairs/clusters showed strong bootstrap support, consistent with close sequence similarity among those taxa in this dataset. Notably, *Tuta absoluta* (OQ201153.1) and *Phthorimaea operculella* (PP801004.1) formed a highly supported pair (bootstrap = 100). A similarly strong pairing was observed for *Bombyx mori* (EF488994.2) and *Bombyx mandarina* (FJ265741.1) (bootstrap = 100), and for *Cydia pomonella* (MF574692.1) with *Grapholita molesta* (MW538482.1) (bootstrap = 100). Within the Heliothinae-containing portion of the tree, *Helicoverpa armigera* (PP163258.1) clustered with *Heliothis virescens* (AF140021.1) with maximal support (bootstrap = 100), whereas another *H. armigera* entry (AY371318.1) clustered near *Athetis lepigone* (OR373042.1) with moderate support (bootstrap = 52), illustrating that not all internal splits are equally supported across the sampled sequences.

At deeper levels, several internal nodes exhibited comparatively low bootstrap values (e.g., 13, 7, 42, 57, 19), indicating weaker support for some higher-order relationships among subclades. Nonetheless, parts of the lower portion of the tree were supported by higher bootstrap values, including the clustering of *Spodoptera frugiperda* (OL961821.1) with *Mythimna separata* (MH346413.1) (bootstrap = 100) and an associated deeper node marked with bootstrap values 98 and 63 in that region of the tree (Fig. 3). Collectively,

the topology highlights a mixture of highly supported terminal relationships alongside less well-supported internal branching patterns among the included Lepidoptera sequences.

Broad-scale placement of Plutella xylostella CYP9G2 across insects

When CYP9-related coding sequences from several insect orders were analyzed together (Fig. 4; scale bar = 2 substitutions per site), AB458853.1 (*P. xylostella*) again did not fall within a strongly supported, tightly clustered lepidopteran-only group; instead, it appeared within a central region of the tree where several adjacent internal nodes carry low bootstrap values (including nodes labeled 1 and 7 in the vicinity of the *P. xylostella* branch). This pattern indicates that, in the context of the taxa sampled for Figure 4, the precise local placement of AB458853.1 is weakly supported relative to multiple other terminal clusters shown in the same tree.

Despite these low-support internal relationships, several groupings in Figure 4 are more strongly supported. For example, *Chilo suppressalis* (KF701146.1) clustered with *Spodoptera litura* (GQ465040.1) with moderate-to-high support (bootstrap = 86). A lepidopteran pairing/clade involving *Ephestia elutella* (MW417340.1) and *Ostrinia furnacalis* (MT039805.1) was also supported (bootstrap = 70). Other taxa from non-lepidopteran orders (e.g., Diptera: *Aedes aegypti* AY064093.1, *Drosophila mettleri* AF083945.1, *Bactrocera dorsalis* KT601134.1; Hymenoptera: *Osmia bicornis* MH500623.1; Coleoptera: *Sitophilus oryzae* MN635166.1, *Dendroctonus valens* ON245946.1; Blattodea: *Blattella germanica* AF275640.1) were distributed across the tree, reflecting the breadth of sequence divergence represented (as also indicated by the comparatively large scale bar in Fig. 4).

Overall, Figures 3 and 4 consistently show that while several terminal relationships among closely related taxa are strongly supported (particularly in the Lepidoptera-focused analysis), the immediate branching context of *P. xylostella* CYP9G2 (AB458853.1) is associated with comparatively low bootstrap support in the multi-order reconstruction and is not presented as part of a highly supported, tight terminal pair in the Lepidoptera-focused tree.

Transcriptional responses of CYP321E1 after insecticide exposure

Quantitative RT–qPCR revealed marked treatment- and time-dependent modulation of *CYP321E1* across the three *Plutella xylostella* populations (Table 1). Within each population, one-way ANOVA indicated a significant overall effect of treatment on *CYP321E1* transcript abundance (Arak population: $F\_(4,10) = 204.42$, $p = 1.53 \times 10^{-9}$; Karaj population: $F\_(4,10) = 42.12$, $p = 3.16 \times 10^{-6}$; Qazvin population: $F\_(4,10) = 35.32$, $p = 7.15 \times 10^{-6}$). Post hoc mean separation (lowercase letters in Table 1) delineated population-specific expression profiles.In the Arak population, *CYP321E1* increased from the control baseline (1.01 ± 0.11; a) to 21.70 ± 1.82 at acetamiprid 48 h (b), and further to 68.49 ± 5.23 at acetamiprid 72 h (c). Cypermethrin exposure produced similarly high expression at 48 h (59.49 ± 1.75) and 72 h (50.34 ± 9.78), with both time points assigned to c, indicating no statistically detectable difference between cypermethrin 48 h and 72 h within P1, while both remained separated from the control (a) and from acetamiprid 48 h (b) (Table 1).In the Karaj population, acetamiprid induced *CYP321E1* to 19.61 ± 5.02 at 48 h and 32.10 ± 5.28 at 72 h, with both values classified as b, indicating no significant time-dependent change under acetamiprid within this population. Under cypermethrin, expression reached 26.37 ± 3.94 at 48 h (b) but declined to 8.92 ± 1.63 at 72 h (c), reflecting a statistically distinct 72 h response relative to the treatments grouped as b within P2 (Table 1).In the Qazvin population, the control (1.04 ± 0.20; a) differed from all insecticide treatments. Acetamiprid elicited 33.39 ± 9.13 at 48 h and 17.49 ± 2.97 at 72 h, with both values assigned to b, indicating no statistically detectable difference between these two time points under acetamiprid within P3 according to the table notation. Cypermethrin produced lower mean values at 48 h (9.37 ± 2.95) and 72 h (4.06 ± 0.75), both classified as c, indicating no significant difference between cypermethrin 48 h and 72 h within P3, while both remained separated from the control (a) and from the acetamiprid group (b) (Table 1).

Transcriptional responses of CYP9G2 after insecticide exposure

In contrast to *CYP321E1*, *CYP9G2* exhibited more heterogeneous population-specific response patterns across insecticides and time points (Table 2). One-way ANOVA confirmed a significant treatment effect within each population (Arak population: $F\_(4,10) = 5.00$, $p = 0.0178$; Karaj population: $F\_(4,10) = 7.76$, $p = 0.00410$; Qazvin population: $F\_(4,10) = 47.43$, $p = 2.00 \times 10^{-6}$). Post hoc grouping (letters in Table 2) resolved distinct within-population contrasts.In the Arak population, the control level (1.06 ± 0.26; a) did not differ from acetamiprid at 48 h (1.60 ± 0.45; a) or 72 h (1.90 ± 0.19; a), nor from cypermethrin at 72 h (0.89 ± 0.27; a). By contrast, cypermethrin at 48 h increased expression to 3.50 ± 0.89 and was assigned to b, indicating a significant elevation relative to the conditions grouped as a within P1 (Table 2).In the Karaj population, the control (1.02 ± 0.16; a) and the values observed for acetamiprid at 48 h (2.94 ± 0.82; a) and 72 h (2.43 ± 0.59; a), as well as cypermethrin at 48 h (2.30 ± 0.61; a), were all within the same statistical group. At 72 h, cypermethrin reached 6.58 ± 0.30 and was assigned to b, indicating a significant increase relative to the set of treatments grouped as a in P2 (Table 2).In the Qazvin population, the control (1.01 ± 0.12; a) was separated from all insecticide treatments. Acetamiprid at 48 h (9.16 ± 1.87; b) and 72 h (11.27 ± 1.31; b), together with cypermethrin at 48 h (11.71 ± 0.40; b), shared the same statistical group, indicating comparable induction levels among these treatments within P3. Cypermethrin at 72 h (5.18 ± 0.83) formed a distinct group (c), indicating a statistically separable response relative to both the control (a) and the higher-expression group (b) within this population (Table 2).

Heatmap-based overview of CYP321E1 expression patterns

The $\log_2$ fold-change heatmap for *CYP321E1* highlighted clear population-, insecticide-, and time-dependent differences in transcript responses among the three *Plutella xylostella* populations (Figure 5). As expected from the normalization strategy, the untreated controls for P1 (Arak), P2 (Karaj), and P3 (Qazvin) were centered at $\log_2(FC) = 0.00$. Following acetamiprid exposure at 48 h, *CYP321E1* showed increased expression in all populations (P1/Arak: 4.44; P2/Karaj: 4.29; P3/Qazvin: 5.06). However, the 72 h pattern diverged among populations: expression increased further in P1 (Arak) to 6.10 and in P2 (Karaj) to 5.00, whereas it decreased in P3 (Qazvin) to 4.13. Under cypermethrin, the strongest response at 48 h was observed in P1 (Arak) (5.89), with a slight reduction by 72 h (5.65). In contrast, P2 (Karaj) and P3 (Qazvin) exhibited more pronounced declines from 48 h to 72 h (P2/Karaj: 4.72 to 3.15; P3/Qazvin: 3.23 to 2.04). Overall, the heatmap indicates that the magnitude and persistence of *CYP321E1* induction were greatest in P1 (Arak), whereas P2 (Karaj) and, especially, P3 (Qazvin) showed comparatively lower $\log_2$ fold-change values at 72 h under cypermethrin and a divergent temporal profile under acetamiprid (Figure 5).

Heatmap-based overview of CYP9G2 expression patterns

The heatmap summarizes the relative transcriptional responses of CYP9G2 in three *P. xylostella* field populations—P1 (Arak), P2 (Karaj), and P3 (Qazvin)—following exposure to acetamiprid or cypermethrin at 48 h and 72 h (Figure 6). By definition, the untreated controls were centered at a $\log_2$ fold change of 0.00 across all populations. Across treatments, P3 (Qazvin) consistently showed the strongest CYP9G2 induction, with elevated $\log_2$ fold changes at 48 h (3.20 under acetamiprid; 3.55 under cypermethrin) and remaining high at 72 h (3.49 under acetamiprid; 2.37 under cypermethrin). In contrast, P1 (Arak) showed comparatively modest induction at 48 h (0.68 under acetamiprid; 1.81 under cypermethrin) and a divergence at 72 h, where expression remained slightly increased under acetamiprid (0.93) but shifted below the control level under cypermethrin (−0.17). P2 (Karaj) displayed intermediate responses across treatments, with $\log_2$ fold-change values ranging from 1.20–1.56 at 48 h and increasing under cypermethrin at 72 h (2.72) while remaining more moderate under acetamiprid at 72 h (1.28). Collectively, the heatmap highlights pronounced population-dependent differences in CYP9G2 induction, with the largest and most consistent upregulation observed in P3 (Qazvin) across both insecticides and sampling times (Figure 6).

Discussion

In the lepidopteran CYP321E1 phylogeny (Fig. 1), *Plutella xylostella* CYP321E1 (KC626090.1) clustered most closely with *Hyphantria cunea* (ON032366.1) with modest support (bootstrap =

40), whereas many deeper nodes across the backbone were weakly supported (often ≤16, and sometimes 0). This pattern is consistent with a well-recognized feature of insect cytochrome P450 (CYP) evolution: rapid lineage-specific gene turnover (duplication, loss, and divergence) tends to preserve clearer "terminal" similarity among close relatives while eroding the phylogenetic signal needed to resolve deeper branching among paralog-rich families (Dermauw et al., 2020). In practical terms, the weak internal support in Fig. 1 should not be read as biological absence of relationships; rather, it likely reflects a combination of (i) short effective alignment length after removing ambiguous regions, (ii) saturation of substitutions across older splits, and (iii) the intrinsic difficulty of reconstructing CYP-family histories when paralogy is common and orthology is not guaranteed. These limitations are amplified when using distance-based Neighbor-Joining (NJ), which is computationally efficient but often less robust than model-based approaches (maximum likelihood/Bayesian) for deep, heterogeneous datasets. A constructive implication is that Fig. 1 is most defensible for interpreting *local* placement (nearest-neighbor context) and for hypothesis generation (candidate functional neighborhood), rather than for drawing strong claims about higher-order lepidopteran CYP321 relationships. Importantly, CYP321E1 in *P. xylostella* has been functionally tied to insecticide resistance via RNAi-based evidence under chlorantraniliprole exposure (Hu et al., 2014), making its nearest-neighbor context biologically meaningful: local clustering suggests shared ancestry with other lepidopteran CYPs that may also be engaged in xenobiotic metabolism, even if deeper relationships remain unresolved.

In the broad-scale CYP321E1 phylogeny across insects (Fig. 2), *P. xylostella* CYP321E1 grouped with *Locusta migratoria* and *Leptinotarsa decemlineata* with strong support at the corresponding node (bootstrap = 95), while the deeper split separating major groups showed weaker support (bootstrap = 48). At face value, a high-support multi-order clustering can look surprising, because CYP sequences typically follow both phylogeny and "CYP clan/family" architecture rather than creating stable cross-order clusters for single genes. Two interpretations are plausible and not mutually exclusive. First, this clustering could suggest that the sampled sequences across orders are not strict orthologs, but rather members of a broader CYP lineage (e.g., within the CYP3 clan) that retains sufficient similarity to cluster under NJ when taxon sampling is limited (Dermauw et al., 2020). Second, the pattern may reflect methodological artifacts, such as long-branch attraction, in which rapidly evolving lineages are pulled together by distance methods, especially when the dataset spans broad taxonomic distances and substitution processes vary among lineages (Dermauw et al., 2020). This matters biologically because functional inference from cross-order clustering should be conservative: even if sequences cluster, detoxification phenotypes can evolve convergently via different CYP genes and regulatory routes. Thus, Fig. 2 is best used as a macro-context figure supporting the idea that CYP321E1 sits within a broadly diversified, xenobiotic-relevant CYP landscape—rather than as evidence of a specific, conserved orthologous relationship across orders. A more decisive test would pair expanded sampling (more lepidopteran CYP321 family members and closer relatives), model-based inference, and—critically—functional assays demonstrating shared substrate specificity.

In the lepidopteran CYP9G2 phylogeny (Fig. 3), *P. xylostella* CYP9G2 (AB458853.1) appeared on a distinct terminal branch, and its immediate local placement lacked strong bootstrap annotation, while several other lepidopteran pairs were strongly supported (often bootstrap = 100). This juxtaposition—strong support for some pairs but weak support near the target sequence—fits the notion that CYP9-family genes can be highly divergent even among Lepidoptera, with rapid sequence evolution and frequent duplication creating species-specific branches (Dermauw et al., 2020). In *P. xylostella*, multiple CYP9 genes have been implicated in pyrethroid response, and CYP9G2 has been described among permethrin-inducible CYPs (Bautista et al., 2007). Divergence in CYP9G2 relative to the set of sequences included in Fig. 3 could therefore reflect (i) genuine sequence novelty within *P. xylostella* (e.g., an expanded or specialized CYP9 lineage), (ii) incomplete representation of the closest CYP9G2-like sequences in the dataset, or (iii) mixed inclusion of paralogs labeled as "CYP9-like" across taxa. Functionally, this matters because CYP9 genes are classic contributors to metabolic resistance, yet their sequence divergence

can be driven by selection on substrate recognition sites. In other words, the distinct placement of *P. xylostella* CYP9G2 is consistent with a detoxification role shaped both ecologically and chemically (Liu et al., 2015).

In the broad-scale CYP9G2 phylogeny (Fig. 4), AB458853.1 again fell in a region with very low bootstrap values nearby (nodes labeled 1 and 7), while several other clusters were moderately supported (e.g., *Chilo suppressalis* with *Spodoptera litura* at bootstrap = 86). The large divergence scale bar (2 substitutions per site) and the weak internal support around the *P. xylostella* branch suggest that the multi-order dataset captures extreme sequence heterogeneity and probable saturation across many sites—conditions under which precise branching positions become unstable and method-sensitive. This observation reinforces two points relevant to resistance biology. First, the CYP9 landscape is best viewed as a "functional reservoir" in which detoxification competence can emerge through multiple gene solutions, rather than as a neatly orthologous system across orders (Dermauw et al., 2020; Liu et al., 2015). Second, weak backbone support argues against overinterpreting AB458853.1's cross-order neighborhood; instead, functional inference should be anchored in expression patterns under insecticide challenge and, ideally, direct metabolic evidence. For CYP9 genes, validations commonly include synergism assays with P450 inhibitors, heterologous expression, and RNAi/CRISPR assays (Liu et al., 2015).

CYP321E1 expression was strongly and significantly induced after insecticide exposure, with the Arak population increasing from 1.01 ± 0.11 (control) to 21.70 ± 1.82 at acetamiprid 48 h and to 68.49 ± 5.23 at acetamiprid 72 h; under cypermethrin, Arak reached 59.49 ± 1.75 (48 h) and 50.34 ± 9.78 (72 h). This magnitude—tens of fold above baseline—strongly suggests a transcriptionally mobilized detoxification response rather than a minor stress fluctuation. Such large inductions are typical of CYP genes that lie downstream of xenobiotic-sensing regulatory circuits and participate in metabolic resistance, particularly under repeated selection in field populations (Liu et al., 2015; Ye et al., 2022). In *P. xylostella*, CYP321E1 has already been linked to insecticide resistance using RNA interference approaches (Hu et al., 2014), and transcriptome-level studies have repeatedly reported broad upregulation of detoxification genes in resistant strains, including CYPs and their electron-transfer partners (Lin et al., 2013; Chen & Zhang, 2015). Mechanistically, the strong CYP321E1 induction in Arak under *both* acetamiprid (a neonicotinoid) and cypermethrin (a pyrethroid) is especially informative: it points to either broad substrate potential or participation in a general xenobiotic response module that supports cross-resistance. Cross-resistance mediated by P450s is a recurrent theme in pest management because elevated oxidative metabolism can reduce susceptibility across multiple insecticide classes (Ye et al., 2022). From an applied perspective, Arak's sustained high expression at 72 h—particularly the continued rise under acetamiprid—suggests that the population may carry regulatory architecture favoring prolonged induction, which can increase the probability that larvae remain protected beyond the early exposure window, potentially affecting delayed mortality and field control outcomes.

In the Karaj population, CYP321E1 increased to 19.61 ± 5.02 (acetamiprid 48 h) and 32.10 ± 5.28 (acetamiprid 72 h), whereas under cypermethrin it increased to 26.37 ± 3.94 at 48 h and then dropped to 8.92 ± 1.63 at 72 h. This pattern implies a more transient response to cypermethrin in Karaj: strong early induction followed by attenuation. One biological explanation is that early CYP321E1 upregulation is sufficient to metabolize a portion of the insecticide load, after which negative feedback, energetic costs, or shifting physiological priorities reduce transcription. Such time-dependent "pulse-and-decline" behavior is consistent with inducible detoxification systems that are costly to maintain at peak expression (Liu et al., 2015). A second explanation is that cypermethrin-induced transcriptional activation in Karaj is mediated by signaling that diminishes after initial stress (e.g., reduced xenobiotic presence due to excretion/metabolism), whereas acetamiprid sustains a more stable induction. This is plausible because insecticides differ in uptake kinetics, persistence, and the extent to which they generate secondary oxidative or membrane stress, all of which can affect transcriptional dynamics. Comparative work across pests supports the idea that neonicotinoids and pyrethroids can drive distinct temporal programs of detox gene induction, and that resistance phenotypes often reflect not just which genes respond, but *how long*

the response persists (Ullah et al., 2020; Zhou et al., 2020).

In the Qazvin population, CYP321E1 rose from 1.04 ± 0.20 (control) to 33.39 ± 9.13 at acetamiprid 48 h and 17.49 ± 2.97 at acetamiprid 72 h, while cypermethrin produced lower values (9.37 ± 2.95 at 48 h and 4.06 ± 0.75 at 72 h). Qazvin therefore shows an acetamiprid-skewed profile for CYP321E1 (stronger under neonicotinoid than pyrethroid), with evidence of attenuation by 72 h. This response contrasts sharply with Arak, where CYP321E1 remained very high under both insecticides. Such population divergence is a hallmark of field resistance evolution: different pesticide use histories and genetic backgrounds can select for distinct resistance architectures, including different "favorite" detox genes and distinct regulatory settings (Banazeer et al., 2022). In Qazvin, the weaker CYP321E1 response under cypermethrin suggests that pyrethroid detoxification may rely more heavily on other CYP families (including CYP9 members) or on alternative enzyme systems (e.g., esterases), whereas acetamiprid challenge recruits CYP321E1 more strongly. The key implication is that "one-gene monitoring" is rarely sufficient across regions: even within one country, resistance biomarkers can be geographically contingent.

CYP9G2 responses were more heterogeneous, with Arak showing a significant increase only under cypermethrin at 48 h (3.50 ± 0.89) while remaining near baseline under other treatments; Karaj showing a significant rise under cypermethrin at 72 h (6.58 ± 0.30) but not at earlier time points; and Qazvin showing strong induction across treatments (acetamiprid 48 h = 9.16 ± 1.87; acetamiprid 72 h = 11.27 ± 1.31; cypermethrin 48 h = 11.71 ± 0.40; cypermethrin 72 h = 5.18 ± 0.83). The clearest inference is that CYP9G2 is most consistently engaged in Qazvin, and that its induction profile aligns with a broad xenobiotic response that spans both neonicotinoid and pyrethroid exposure. CYP9-family genes in *P. xylostella* have long been associated with pyrethroid inducibility (Bautista et al., 2007), so the strong cypermethrin response in Qazvin is unsurprising; however, the similarly high induction under acetamiprid points toward cross-class responsiveness or shared regulatory control. In other pests, acetamiprid resistance and cross-resistance have been linked to CYP-mediated detoxification and upregulation of multiple P450 genes, with functional evidence demonstrating that specific CYPs contribute to resistance phenotypes (Ullah et al., 2020; Zhou et al., 2020). While those studies are not *P. xylostella*-specific, they strengthen a mechanistic narrative: high CYP9G2 induction under acetamiprid may indicate that Qazvin larvae have evolved a P450-centered resistance module with broader substrate capacity or shared upstream regulation.

The CYP321E1 heatmap (Fig. 5) showed strong $\log_2$ fold-change values across all populations under acetamiprid at 48 h (Arak 4.44; Karaj 4.29; Qazvin 5.06), but divergent 72 h dynamics, with Arak and Karaj increasing further (6.10 and 5.00) while Qazvin declined (4.13); under cypermethrin, Arak remained high (5.89 → 5.65), whereas Karaj and Qazvin declined more sharply (4.72 → 3.15; 3.23 → 2.04). This visualization integrates and clarifies the table-level findings by revealing response *shape* (persistence vs decay) in a compact form. Biologically, persistence is often the difference between tolerance and failure under repeated or prolonged exposure. A sustained induction (as in Arak) can reflect either strong inducible regulation or partial constitutive elevation that enables faster and higher transcriptional output upon challenge (Liu et al., 2015). Declining profiles (as in Karaj and Qazvin under cypermethrin) could reflect detoxification completion, but they can also signal regulatory constraints—possibly because prolonged high CYP expression imposes metabolic burdens (e.g., NADPH demand, oxidative byproducts). Fitness costs are frequently observed in insecticide-resistant populations and can shape the stability of resistance alleles in the absence of insecticide (Banazeer et al., 2022; Ullah et al., 2020). From a management perspective, the heatmap suggests that Arak may be at higher risk of operational control failures with both insecticides, as both magnitude and persistence are elevated. This aligns with the broader literature that emphasizes regional heterogeneity and the need for resistance surveillance tailored to local populations rather than extrapolated from a single site (Furlong et al., 2013; Wang et al., 2021).

The CYP9G2 heatmap (Fig. 6) emphasized Qazvin's consistently strongest induction ($\log_2$ fold-change 3.20–3.55 at 48 h and 2.37–3.49 at 72 h), contrasted with modest or inconsistent changes in Arak (including a shift below baseline under cypermethrin at 72 h, −0.17) and intermediate,

treatment-specific responses in Karaj (notably 2.72 under cypermethrin at 72 h). Two mechanistic interpretations are particularly relevant. First, Qazvin may have evolved a CYP9G2-centered detoxification axis that is activated across chemical classes, consistent with P450-driven cross-resistance patterns described in multiple agricultural pests (Ye et al., 2022; Zhou et al., 2020). Second, the Arak profile hints at potential pathway partitioning: Arak relies heavily on CYP321E1 (high induction), whereas CYP9G2 is not consistently induced and may even be downregulated at later time points under cypermethrin. This kind of "division of labor" across CYP genes is consistent with modern views of metabolic resistance as a network property—multiple CYPs can contribute, but populations differ in which nodes are dominant and how they are regulated (Liu et al., 2015; Dermauw et al., 2020). Such divergence also helps explain why field monitoring based on one candidate gene can yield inconsistent predictive power across regions. Consequently, the most valuable next step is to convert these transcriptional signatures into functional evidence: (i) synergist bioassays (e.g., piperonyl butoxide) to test P450 contribution at the phenotype level, (ii) heterologous expression to test whether CYP321E1 and CYP9G2 metabolize acetamiprid/cypermethrin directly, and (iii) RNAi/CRISPR perturbation to assess causal contribution—approaches that have been informative for CYP-mediated resistance in *P. xylostella* and other pests (Hu et al., 2014; Liu et al., 2015; Ullah et al., 2020).

Finally, the study design explicitly paired RT–qPCR responses with insecticide bioassays at 48 h and 72 h, and the results demonstrate statistically significant treatment effects within each population for both genes. This is a strength because it aligns molecular readouts with ecologically meaningful exposure windows. However, transcription alone cannot distinguish whether induction is *defensive detoxification* or a broader stress response secondary to intoxication. Detoxification interpretation becomes most compelling when expression correlates with susceptibility metrics (LC_{50} or survival) and when functional assays confirm metabolism (Liu et al., 2015; Ye et al., 2022). Where such linkage is not yet fully established, the cautious, publication-ready framing is that CYP321E1 and CYP9G2 are strong candidate biomarkers whose population-specific expression patterns support a working model of differential metabolic resistance architecture among Iranian *P. xylostella* populations. My view is that the most impactful future direction is to expand from "two-gene diagnostics" toward a small, validated panel (CYPs + reductase partners + a regulatory marker), because resistance in DBM is repeatedly shown to be multi-mechanistic and regionally variable (Banazeer et al., 2022; Furlong et al., 2013; Lin et al., 2013).

Conclusion

This study places two resistance-relevant P450 genes into a comparative evolutionary framework and then demonstrates strong, population-specific transcriptional responses to two widely used insecticides. Phylogenetic analyses show that terminal groupings are clearer than deeper relationships, consistent with rapid CYP diversification. At the expression level, CYP321E1 exhibited exceptionally strong induction in the Arak population under both acetamiprid and cypermethrin, while Karaj and Qazvin showed more transient or insecticide-skewed patterns. CYP9G2 responses were notably heterogeneous, with Qazvin displaying robust induction across insecticides and time points, suggesting a distinct metabolic resistance configuration compared with Arak, where CYP321E1 dominated. Together, these findings support a model in which geographically separated DBM populations can evolve different "detoxification solutions," emphasizing the need for region-specific resistance monitoring and management. The most decisive next steps are functional validation (synergist assays, heterologous metabolism tests, and gene knockdown/knockout) and integration of expression signatures with toxicity metrics to build predictive molecular diagnostics.

Acknowledgements

The University of Zabol financially supported this research. We sincerely thank Mr. Derakhshan (Plant Protection Manager of Qazvin Province), Mr. Shahsavari (Plant Protection Expert of Qazvin Province), Dr. Samadipour (Plant Protection Manager of Alborz Province), and Mr. Ghadami (Plant Protection Manager of Markazi Province) for their invaluable assistance in locating cabbage fields infested with the pest.

Table 1-Relative expression of a target cytochrome P450 gene (CYP321E1) in three *Plutella xylostella* populations following acetamiprid and cypermethrin exposure.

Treatment	Arak	Karaj	Qazvin
Control	1.01 ± 0.11 a	1.07 ± 0.26 a	1.04 ± 0.20 a
Acetamiprid 48	21.70 ± 1.82 b	19.61 ± 5.02 b	33.39 ± 9.13 b
Acetamiprid 72	68.49 ± 5.23 c	32.10 ± 5.28 b	17.49 ± 2.97 b
Cypermethrin 48	59.49 ± 1.75 c	26.37 ± 3.94 b	9.37 ± 2.95 c
Cypermethrin 72	50.34 ± 9.78 c	8.92 ± 1.63 c	4.06 ± 0.75 c

Values are presented as mean ± SE of relative transcript abundance (fold-change) for the Arak, Karaj, and Qazvin populations under untreated control conditions and at 48 h and 72 h after exposure to acetamiprid or cypermethrin. Within each population (column), means followed by the same lowercase letter are not significantly different, whereas different letters indicate significant differences among treatments/time points ($p < 0.05$; as indicated by the lettering in the table).

Table 2– Relative expression of a target cytochrome P450 gene (CYP9G2) in three *Plutella xylostella* populations following acetamiprid and cypermethrin exposure.

Treatment	Arak	Karaj	Qazvin
Control	1.06 ± 0.26 a	1.02 ± 0.16 a	1.01 ± 0.12 a
Acetamiprid 48	1.60 ± 0.45 a	2.94 ± 0.82 a	9.16 ± 1.87 b
Acetamiprid 72	1.90 ± 0.19 a	2.43 ± 0.59 a	11.27 ± 1.31 b
Cypermethrin 48	3.50 ± 0.89 b	2.30 ± 0.61 a	11.71 ± 0.40 b
Cypermethrin 72	0.89 ± 0.27 a	6.58 ± 0.30 b	5.18 ± 0.83 c

Values are presented as mean ± SE of relative CYP9G2 transcript abundance (fold-change) for the Arak, Karaj, and Qazvin populations under untreated control conditions and at 48 h and 72 h after exposure to acetamiprid or cypermethrin. Within each population (column), means followed by the same lowercase letter are not significantly different, whereas different letters indicate significant differences among treatments/time points ($p < 0.05$; as indicated by the lettering in the table).

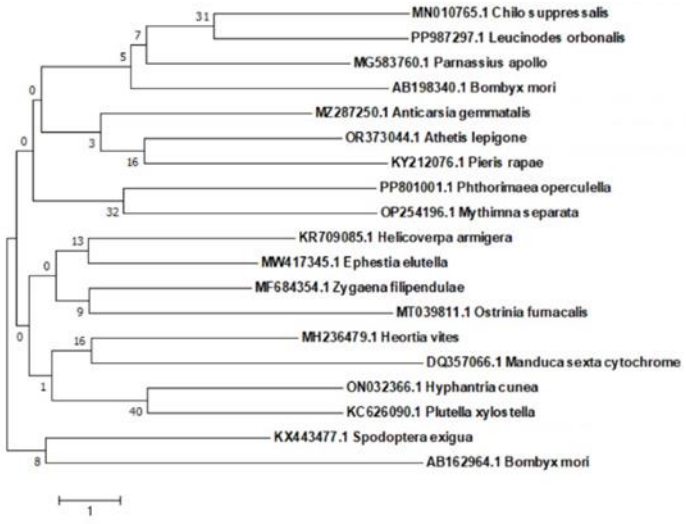

Figure. 1- Molecular phylogenetic analysis of lepidopteran cytochrome P450 coding sequences, highlighting the position of *Plutella xylostella* CYP321E1.

The phylogenetic analysis included the following insect species (GenBank accession numbers in parentheses): *Chilo suppressalis* (MN010765.1), *Spodoptera exigua* (KX443477.1), *Apis mellifera* (DQ244074.1), *Aedes aegypti* (AY947549.1), *Bombyx mori* (AB198340.1), *Anopheles gambiae* (KF656700.1), *Sitophilus oryzae* (MN635144.1), *Drosophila melanogaster* (AY138853.1), *Helicoverpa armigera* (KR709085.1), *Bemisia tabaci* (PP239341.1), *Tenebrio molitor* (KP859376.1), *Locusta migratoria* (KY009922.1), *Plutella xylostella* (KC626090.1), and *Leptinotarsa decemlineata* (KF044272.1). Numbers at nodes indicate bootstrap support values calculated from 10000 replicates; the scale bar represents 1 unit of sequence divergence per site.

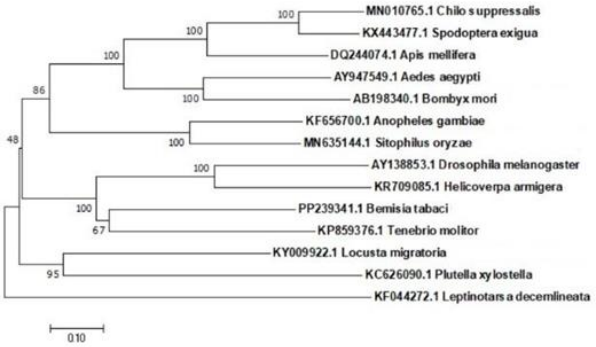

Figure. 2_ Molecular phylogenetic analysis of insect cytochrome P450 coding sequences, highlighting the position of *Plutella xylostella* CYP321E1.

The phylogenetic analysis included the following insect species (GenBank accession numbers in parentheses): *Chilo suppressalis* (MN010765.1), *Spodoptera exigua* (KX443477.1), *Apis mellifera* (DQ244074.1), *Aedes aegypti* (AY947549.1), *Bombyx mori* (AB198340.1), *Anopheles gambiae* (KF656700.1), *Sitophilus oryzae* (MN635144.1), *Drosophila melanogaster* (AY138853.1), *Helicoverpa armigera* (KR709085.1), *Bemisia tabaci* (PP239341.1), *Tenebrio molitor* (KP859376.1), *Locusta migratoria* (KY009922.1), *Plutella xylostella* (KC626090.1), and *Leptinotarsa decemlineata* (KF044272.1). Numbers at nodes indicate bootstrap support values calculated from 10000 replicates.

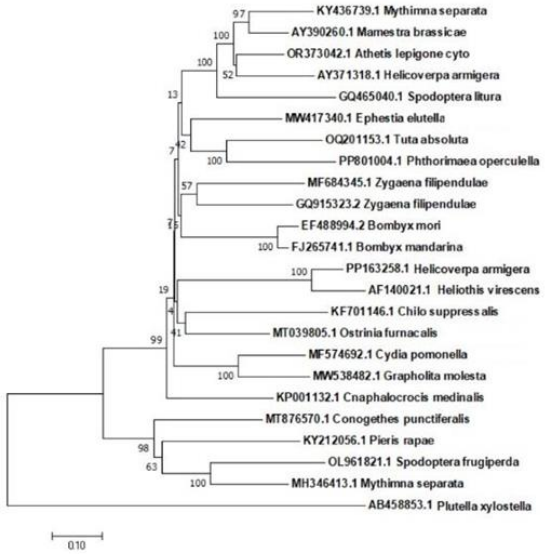

Figure. 3- Molecular phylogenetic analysis of lepidopteran cytochrome P450 coding sequences, highlighting the position of *Plutella xylostella* CYP9G2.

The phylogenetic analysis incorporated the following lepidopteran species (GenBank accession numbers in parentheses): Mythimna separata (KY436739.1), Mamestra brassicae (AY390260.1), Athetis lepigone (OR373042.1), Helicoverpa armigera (AY371318.1 and PP163258.1), Spodoptera litura (GQ465040.1), Ephestia elutella (MW417340.1), Tuta absoluta (OQ201153.1), Phthorimaea operculella (PP801004.1), Zygaena filipendulae (MF684345.1 and GQ915323.2), Bombyx mori (EF488994.2), Bombyx mandarina (FJ265741.1), Heliothis virescens (AF140021.1), Chilo suppressalis (KF701146.1), Ostrinia furnacalis (MT039805.1), Cydia pomonella (MF574692.1), Grapholita molesta (MW538482.1), Cnaphalocrocis medinalis (KP001132.1), Conogethes punctiferalis (MT876570.1), Pieris rapae (KY212056.1), Spodoptera frugiperda (OL961821.1), and Plutella xylostella (AB458853.1). Numbers at nodes indicate bootstrap support values calculated from 10000 replicates.

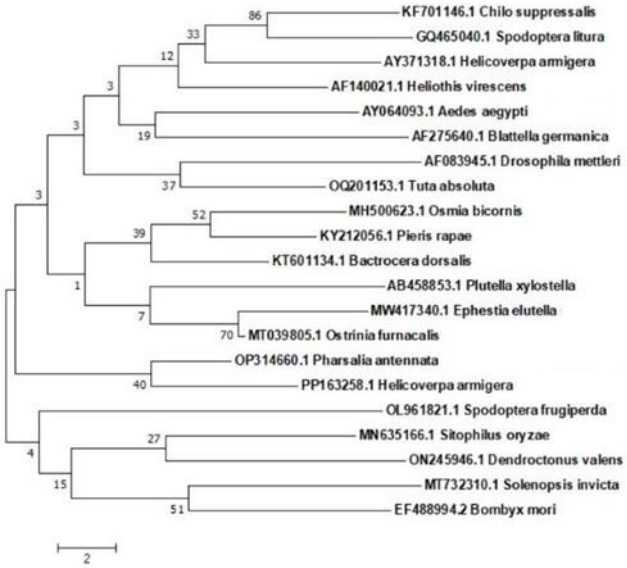

Figure. 4- Molecular phylogenetic analysis of insect cytochrome P450 coding sequences, highlighting the position of *Plutella xylostella* CYP9G2.

The phylogenetic analysis for Figure 4 included the following species and sequences: *Chilo*

suppressalis (KF701146.1), *Spodoptera litura* (GQ465040.1), *Helicoverpa armigera* (AY371318.1 and PP163258.1), *Heliothis virescens* (AF140021.1), *Aedes aegypti* (AY064093.1), *Blattella germanica* (AF275640.1), *Drosophila mettleri* (AF083945.1), *Tuta absoluta* (OQ201153.1), *Osmia bicornis* (MH500623.1), *Pieris rapae* (KY212056.1), *Bactrocera dorsalis* (KT601134.1), *Plutella xylostella* (AB458853.1), *Ephestia elutella* (MW417340.1), *Ostrinia furnacalis* (MT039805.1), *Pharsalia antennata* (OP314660.1), *Spodoptera frugiperda* (OL961821.1), *Sitophilus oryzae* (MN635146.1), *Dendroctonus valens* (ON245946.1), *Solenopsis invicta* (MT732310.1), and *Bombyx mori* (EF488994.2). Numbers at nodes indicate bootstrap support values calculated from 10000 replicates.

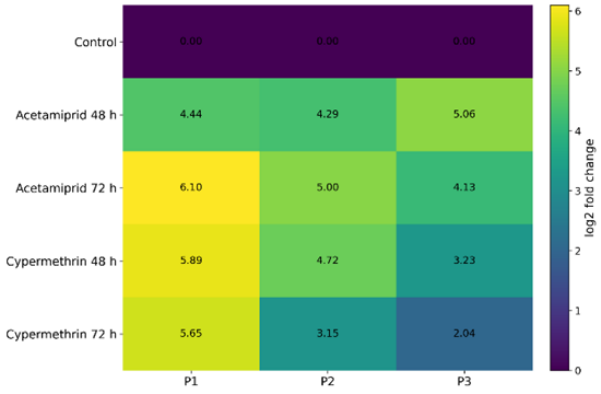

Figure. 5-Heatmap of *CYP321E1* expression responses to insecticide exposure in three field populations of *Plutella xylostella* .

Relative transcript abundance was quantified by RT–qPCR at 48 h and 72 h after exposure to acetamiprid or cypermethrin in populations P1 (Arak), P2 (Karaj), and P3 (Qazvin). Expression was normalized to the reference gene *actin* and calculated using the 2^−ΔΔCt method, with the untreated control from the corresponding population used as the calibrator. Heatmap colors represent $\log_2$-transformed fold-change values; consequently, the control condition is $\log_2(1) = 0$ and is displayed as 0.00. Cell annotations indicate the $\log_2$(fold-change) values used for visualization.

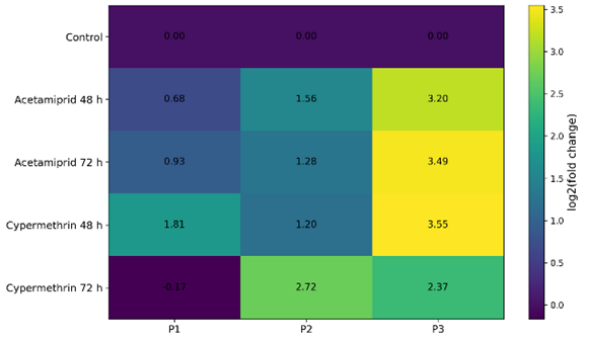

Figure. 6- Heatmap of *CYP9G2* expression responses to insecticide exposure in three field populations of *Plutella xylostella* .

Relative transcript abundance was quantified by RT–qPCR at 48 h and 72 h after exposure to acetamiprid or cypermethrin in populations P1 (Arak), P2 (Karaj), and P3 (Qazvin). Expression was normalized to the reference gene *actin* and calculated using the 2^−ΔΔCt method, with the untreated control from the corresponding population used as the calibrator. Heatmap colors represent $\log_2$-transformed fold-change values; consequently, the control condition is $\log_2(1) = 0$ and is displayed as 0.00. Cell annotations indicate the $\log_2$(fold-change) values used for visualization.

References (Alphabetic Sort)

Alborzi, Z., Amiri, A., Piulachs, M. D., & Bandani, A. R. (2025). Tissue-specific transcriptomic and endocrine signatures of obligatory reproductive diapause in Eurygaster integriceps. Scientific Reports 15(1): 1-17.

Amiri, A., Bandani, A. R. (2013). Comparison of energy reserves in prediapause and diapausing adult Sunn pest, Eurygaster integriceps Puton (Hemiptera: Scutelleridae). Journal Journal of Agricultural Science and Technology, 15 (3): 435-444.

Amiri, A., Bandani, A. R., & Alizadeh, H. (2015). Molecular identification of cysteine and trypsin protease, effect of different hosts on protease expression, and rnai mediated silencing of cysteine protease gene in the sunn pest. Archives of insect biochemistry and physiology, 91(4), 189-209.

Banazeer, A., Afzal, M. B. S., Hassan, S., Ijaz, M., Shad, S. A., & Serrão, J. E. (2022). Status of insecticide resistance in Plutella xylostella (Linnaeus)(Lepidoptera: Plutellidae) from 1997 to 2019: cross-resistance, genetics, biological costs, underlying mechanisms, and implications for management. Phytoparasitica, 50(2), 465-485.

Bautista, M. A. M., Tanaka, T., & Miyata, T. (2007). Identification of permethrin-inducible cytochrome P450s from the diamondback moth, Plutella xylostella (L.) and the possibility of involvement in permethrin resistance. Pesticide Biochemistry and Physiology, 87(1), 85-93.

Casida, J. E., & Durkin, K. A. (2013). Neuroactive insecticides: targets, selectivity, resistance, and secondary effects. Annual review of entomology, 58(1), 99-117.

Chen, X. E., & Zhang, Y. (2015). Identification and characterization of NADPH-dependent cytochrome P450 reductase gene and cytochrome b5 gene from Plutella xylostella: Possible involvement in resistance to beta-cypermethrin. Gene, 558(2), 208-214.

Dermauw, W., Van Leeuwen, T., & Feyereisen, R. (2020). Diversity and evolution of the P450 family in arthropods. Insect biochemistry and molecular biology, 127, 103490.

Farahani, S., Bandani, A. R., & Amiri, A. (2020).Toxicity and repellency effects of three essential oils on two populations of Tetranychus urticae (Acari: Tetranychidae). Persian Journal of Acarology 9 (1): 67-81.

Furlong, M. J., Wright, D. J., & Dosdall, L. M. (2013). Diamondback moth ecology and management: problems, progress, and prospects. Annual review of entomology, 58(1), 517-541.

Hu, Z. D. S. Q., Lin, Q., Chen, H., Li, Z., Yin, F., & Feng, X. (2014). Identification of a novel cytochrome P450 gene, CYP321E1 from the diamondback moth, Plutella xylostella (L.) and RNA interference to evaluate its role in chlorantraniliprole resistance. Bulletin of Entomological Research, 104(6), 716-723.

Lin, Q., Jin, F., Hu, Z., Chen, H., Yin, F., Li, Z., ... & Feng, X. (2013). Transcriptome analysis of chlorantraniliprole resistance development in the diamondback moth Plutella xylostella. PLoS One, 8(8), e72314.

Liu, N., Li, M., Gong, Y., Liu, F., & Li, T. (2015). Cytochrome P450s–Their expression, regulation, and role in insecticide resistance. Pesticide biochemistry and physiology, 120, 77-81.

Nauen, R., Bass, C., Feyereisen, R., & Vontas, J. (2022). The role of cytochrome P450s in insect toxicology and resistance. Annual Review of Entomology, 67(1), 105-124.

Rahmani, S., & Bandani, A. R. (2021). A gene silencing of V-ATPase subunit A interferes with survival and development of the tomato leafminer, Tuta absoluta. Archives of Insect Physiology and Biochemistry, 106(1):e21753.

Schmittgen, T. D., & Livak, K. J. (2008). Analyzing real-time PCR data by the comparative CT method. Nature protocols, 3(6), 1101-1108.

Soderlund, D. M. (2008). Pyrethroids, knockdown resistance and sodium channels. Pest Management Science: formerly Pesticide Science, 64(6), 610-616.

Sparks, T. C., & Nauen, R. (2015). IRAC: Mode of action classification and insecticide resistance management. Pesticide biochemistry and physiology, 121, 122-128.

Ullah, F., Gul, H., Tariq, K., Desneux, N., Gao, X., & Song, D. (2020). Functional analysis of cytochrome P450 genes linked with acetamiprid resistance in melon aphid, Aphis gossypii. Pesticide Biochemistry and Physiology, 170, 104687.

Wang, J., Zheng, X., Yuan, J., Wang, S., Xu, B., Wang, S., ... & Wu, Q. (2021). Insecticide resistance monitoring of the diamondback moth (Lepidoptera: Plutellidae) populations in China. Journal of Economic Entomology, 114(3), 1282-1290.

Ye, M., Nayak, B., Xiong, L., Xie, C., Dong, Y., You, M., ... & You, S. (2022). The role of insect cytochrome P450s in mediating insecticide resistance. Agriculture, 12(1), 53.

You, M., Yue, Z., He, W., Yang, X., Yang, G., Xie, M., ... & Wang, J. (2013). A heterozygous moth genome provides insights into herbivory and detoxification. Nature genetics, 45(2), 220-225.

Yu, L., Tang, W., He, W., Ma, X., Vasseur, L., Baxter, S. W., ... & You, M. (2015). Characterization and expression of the cytochrome P450 gene family in diamondback moth, Plutella xylostella (L.). Scientific Reports, 5(1), 8952.

Zhou, C. S., Cao, Q., Li, G. Z., & Ma, D. Y. (2020). Role of several cytochrome P450s in the resistance and cross-resistance against imidacloprid and acetamiprid of Bemisia tabaci (Hemiptera: Aleyrodidae) MEAM1 cryptic species in Xinjiang, China. Pesticide Biochemistry and Physiology, 163, 209-215.